Some improved geometries for Josephson-junction investigations of the order-parameter symmetry in high-T_c superconductors

R. A. Klemm
Materials Science Division, Argonne National Laboratory, Argonne, Illinois 60439
(Received 19 July 1996)

We propose two new geometries for Josephson junction experiments between the edge of an orthorhombic, untwinned single-crystal high-T_c superconductor, assumed to have an order parameter of the mixed $s \pm d_{x^2-y^2}$ variety, and a conventional, s-wave superconductor. The first geometry is a straight-edge Josephson junction cut at an angle ϕ_0 with respect to the a-axis edge of a high-T_c crystal. We studied the effects of a regular array of a/b steps comprising the edge upon the $I_c(B)$ pattern for different ϕ_0 values. Varying ϕ_0 can elucidate the locations of any purported order-parameter nodes. The second geometry is a disk cut from a high-T_c single crystal, with a Josephson junction formed on the edge, centered at ϕ_0, with an angular width of $\Delta\phi$. The case $\Delta\phi=\pi$ is nearly free of systematic flux trapping problems, and is shown to be particularly important in quantifying the precise amount of s/d order-parameter mixing. Smaller $\Delta\phi$ values can also be useful in locating the purported order-parameter nodes. [S0163-1829(97)01105-3]

I. INTRODUCTION

Recently, there have been a number of experiments purporting to determine the orbital symmetry of the superconducting order parameter in high-T_c superconductors (HTCS's). There are several classes of such experiments, but those which have generally been regarded as being the most definitive all fall in the class of Josephson-junction experiments on $YBa_2Cu_3O_{7-\delta}$ (YBCO).[1–12]

These experiments have focused upon Josephson-junction interferometry, which is rather sensitive to phase changes of the superconducting order parameter. A number of YBCO-YBCO grain boundary experiments[7,8] and YBCO/Pb interferometry experiments,[9–12] if taken at face value, apparently give evidence for an order parameter containing both plus and minus signs, as might be expected if the order parameter had the $d_{x^2-y^2}$ form $\Delta_d\cos(2\phi)$. Other grain boundary experiments were consistent with purely s-wave, superconductivity,[6] with a constant order parameter Δ_s.

In addition, single c-axis and ab-plane Josephson-junction experiments between YBCO and Pb have given strong evidence that the order parameter is either s wave or a mixture of s and d waves, with at least a very substantial s-wave component.[1–5] Whether this s-wave component is larger or smaller than the purported d-wave component Δ_d has not been established in any systematic way.

Unfortunately, all of the experiments claiming to provide evidence for d-wave superconductivity are flawed by geometry, magnetic impurities due to oxygen stoichiometry inhomogeneities at the grain boundaries, self-field extrapolation problems, and/or flux trapping problems, etc. In particular, the early experiments of Refs. 10 and 11 were flawed by possible corner flux-trapping effects,[13] and have since been shown experimentally[14] to be ambiguous, the observed phase shifts being completely indistinguishable from those obtained from the usual self-field effects.[15] In addition, the observation of anomalously large faceting of the YBCO-YBCO grain boundary junctions[16–18] and the associated large amount of oxygen stoichiometry and critical current variations[16,19] of the particular type used in the tricrystal ring experiments involving YBCO (Ref. 7) have raised many questions regarding the reliability of those experiments.[20] Until very recently, the experiment thought by many to be the most reliable evidence for d-wave superconductivity was the YBCO/Pb superconducting quantum interference device (SQUID) experiments,[9] in which reversing the currents and fields also gave strong evidence for a time-reversal-invariant state, eliminating such s/d mixings as the $s+id$ state, which breaks time-reversal invariance. In more recent experiments by the same group,[20] however, it was shown that while the time reversibility was always maintained, the s or d-wave nature of the results was unreliable, with the new results actually being completely consistent with an order parameter that was *odd* under π rotations, such as for the p-wave polar state, and *inconsistent* with any other order parameter. The most likely explanation of these experiments is that there were some serious, as yet unexplained problems with the Ar-ion milling angles used to prepare the YBCO/Pb SQUID junctions.

More recently, the corner Josephson-junction experiments[12] have been shown to give the magnetic induction **B** dependences of the critical current I_c that are indistinguishable from those expected from a monopole flux trapped at the sample corners, the center of the junction, and lying in the ab plane.[21] Corner effects such as this are well known,[22–24] and were shown to give spurious π periodicities with d-wave-like $\pi/2$ subharmonicities in transverse magnetization experiments on samples with corners.[24,25] Such spurious behaviors are completely absent in disk-shaped samples.[24,26] They are the most likely explanation[24] of the magnetothermal resistance anisotropy observed in square YBCO samples.[27]

Although many scientists favoring the d-wave model claimed to be able to explain the c-axis Josephson-junction experiments[1–5] by tunneling into the ab plane at etch pits, such oversimplified notions are really incorrect, as they would certainly not lead to the observed near-perfect Fraun-

0163-1829/97/55(5)/3249(9)/$10.00

hofer diffraction patterns with nodal spacings precisely tuned to the measured penetration depth of the YBCO, as observed. Although the $s+id$ state appears to be strongly at odds with the experiments of the Maryland group,[9,14,20] it also has great difficulty in explaining the extremely narrow widths of the Fiske modes observed in c-axis YBCO/Pb Josephson junctions.[1,4] Hence, these c-axis Josephson-junction experiments really must be taken seriously. These experiments provide very strong evidence that there is indeed an s-wave component to the order parameter. In view of the most recent experiments on the the c-axis face of untwinned single crystals of YBCO and on the ab edges of highly twinned single crystals of YBCO,[2,3,5] it is now evident that the s-wave component comprises a *substantial* fraction of the total order parameter. Using comparisons with the SIS' BCS-theory-based calculation of Ambegaokar and Baratoff,[28] these experiments strongly suggest that the *lower limit* upon the s-wave component of the order parameter is 30% of the total. In addition, the nonobservation of any $\pi/2$ periodicitiy in transverse magnetization experiments[24] also provides evidence for an *absence* of any nodes of the order parameter, so that the s-wave component would have to be larger than the purported d-wave component. Since the first YBCO-YBCO grain boundary experiments[6] gave strong evidence for purely s-wave superconductivity, the question of whether there are nodes of the order parameter has not been settled. In any event, there has to date been no reliable experiment that can actually *measure* the relative amounts of the purported s- and d-wave order parameters. In this paper, we propose two such experiments.

We thus propose two classes of experiments, which are designed to be as free as possible from systematic flux-trapping problems associated with the sample geometry, and do not involve uncontrolled grain boundary faceting. These involve Josephson junctions between a single-crystalline, untwinned HTCS and a conventional superconductor (CS), such as Pb. We presume an orthorhombic HTCS, such as YBCO, is studied. For tetragonal systems, it is generally thought that symmetry considerations prevent the order parameter from being a mixed $s+d$ state, forcing it to be either s or d. In the first set of experiments, the HTCS is cut along a plane parallel to the c axis, and perpendicular to an angle ϕ_0 relative to the a axis. The Josephson junction is then formed with Pb deposited upon the freshly cut edge surface, presumably after depositing a thin interstitial layer of a material such as Ag.[3] In the second set of experiments, the HTCS is cut and polished in the precise shape of a circular disk of radius r_0, and the Pb forms a Josephson-junction centered at an angle ϕ_0 relative to the a axis, and covers an azimuthal arc $r_0\Delta\phi$. In both cases, a scheme is presented for counteracting the large, problematic demagnetization corrections associated with the magnetic field perpendicular to the thin superconducting samples. By varying ϕ_0 with appropriate choices of $\Delta\phi$, a quantitative measure of the amount of s- and d-wave mixing of the order parameter can be precisely determined.

II. HTCS SINGLE CRYSTALS CLEAVED PERPENDICULAR TO THE *ab* PLANE

In this section, we consider the first proposed experimental modification of the Josephson junction experiment of Ref. 12. In this case, we suppose that it is possible to prepare samples of an untwinned HTCS cleaved in a plane containing the c axis, with the normal to the cleave plane making an angle ϕ_0 with respect to the crystal a axis, as pictured in Fig. 1. We label the CS and the HTCS as superconductors 1 and 2, respectively. We first consider the junction prepared on this cleave plane to be perfect, and then we consider the main effects of facets on this cleave plane.

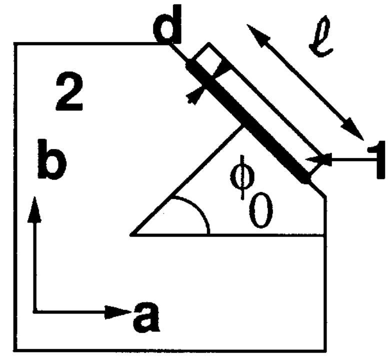

FIG. 1. Schematic top view of a Josephson junction, indicated by the thick bold line, of effective thickness d and length ℓ between a CS (1) placed on a cleave plane normal to the angle ϕ_0 relative to the a axis of a HTSC (2).

A. Perfect straight junctions

In Fig. 1, we illustrate the configuration of the cleave. A Josephson junction is presumed to be prepared upon the cleave face, by depositing a thin layer of thickness t of some ''junction material'' such as Ag, and then a thick layer of a CS, such as Pb. The length of the junction prepared on the cleaved face is then taken to be ℓ, and the total effective field penetration into the SIS' junction (and hence the effective width of the junction) is $d(\phi_0)$ given by

$$d(\phi)=t+\lambda_1+\lambda_{2ab}(\phi), \tag{1}$$

$$\lambda_{2ab}(\phi)=\frac{\lambda_{2a}}{[\sin^2\phi+(\lambda_{2a}/\lambda_{2b})^2\cos^2\phi]^{1/2}}, \tag{2}$$

as pictured in Fig. 1. This is a generalization of the tunneling into the a or b axes considered previously,[29] which was shown to be independent of the particular electronic structure of the HTCS and the CS. In this configuration, it is important that all of the junction be located sufficiently far from the HTCS corners resulting from the cleave, in order to eliminate spurious trapped flux and inhomogenous current distribution problems. Ordinarily, one would suppose that this would imply that the end of the junction should be at least several HTCS penetration depths $\lambda_{2ab}(\phi_0)$ from the corners, but this number probably depends upon the HTCS sample thickness; so it is a good idea to place it yet further from the corners. While it is still possible for magnetic flux to be trapped in the junctions or in the HTCS adjacent to the junction, the particular locations for trapped flux in the junction region are then effectively *random*, rather than nonrandom, as would necessarily occur if the junction were too close to a corner.

We assume the applied magnetic field $\mathbf{H}||\hat{c}$. Of course, the actual magnetic induction $\mathbf{B}$ will not be parallel to $\mathbf{H}$ at the junction, due to the strong demagnetization effects associated with the sample shape, unless one could make the sample effectively very thick. In the Meissner state, $\mathbf{B}$ is everywhere parallel to the sample surface, as $\mathbf{B}\cdot\hat{\mathbf{n}}=0$. For untwinned YBCO, however, the samples are generally much wider than thick, and so demagnetization effects are very strong, and $\mathbf{B}$ is strongly varying in direction over the junction, being essentially normal to the junction at the top and bottom edges of the HTCS sample, and parallel to the junction over the central portion of it.

In Sec. IV, we shall propose an experimental configuration which may prove useful in greatly reducing the strong demagnetization effects, so as to allow for much more quantitative comparisons between theory and experiment. We thus assume that the sample is thick enough so that to zeroth order one can treat $\mathbf{B}||\hat{c}$ over most of the junction. For this idealized straight, perfect junction, it is then straightforward to calculate the flux dependence of the critical current I_c in terms of the normal state resistance R_n. We find[29]

$$eI_cR_n=|G(\phi_0)|, \tag{3}$$

$$G(\phi)\equiv\frac{F_{AB}(\phi)\sin[\pi\Phi(\phi)/\Phi_0]}{\pi\Phi(\phi)/\Phi_0}, \tag{4}$$

$$\Phi(\phi)=B\ell(\phi)d(\phi), \tag{5}$$

$$\ell(\phi)=\ell\cos(\phi_0-\phi), \tag{6}$$

$$F_{AB}(\phi)=\frac{2\Delta_1\Delta_2(\phi)}{|\Delta_1|+|\Delta_2(\phi)|}K\left[\frac{\|\Delta_1|-|\Delta_2(\phi)\|}{|\Delta_1|+|\Delta_2(\phi)|}\right], \tag{7}$$

where e is the electronic charge, $\Phi_0=hc/2e$ is the flux quantum, and $K(z)$ is a complete elliptic integral.

We remark that in preparing the junction, one must be careful to keep the length $\ell(\phi)$ of the junction less than the Josephson length λ_J,[30] or else the critical current distribution will be very nonuniform in the junction, decaying exponentially over λ_J from the junction ends. In this geometry, we have $\lambda_J=[8\pi ed(\phi)J_c]^{-1/2}$, where J_c is the critical current density for junctions from the CS into the ab plane of the HTCS.[30] Assuming an extremely high J_c value of 10^7 A/cm^2, and taking $d(\phi)\sim 200$ nm, we estimate λ_J to be 1 mm. Smaller J_c values lead to correspondingly larger λ_J values. Thus, we require $\ell(\phi)<\lambda_J\approx 1$ mm.

In addition, we have assumed that the critical current density J_c is independent of position along the junction. If it were to vary strongly in position, as can happen when trapped flux is present, Eq. (4) would be modified as in Ref. 31, leading to

$$G(\phi)\to\left|\int_{-\ell(\phi)/2}^{\ell(\phi)/2}\frac{dx}{\ell(\phi)}F_{AB}(\phi,x)\right.$$
$$\left.\times\exp\{2\pi ix\Phi(\phi)/[\ell(\phi)\Phi_0]\}\right|. \tag{8}$$

Thus, one has to be very careful to have a constant critical current distribution, or else in analyzing the data, one will have to try to guess the current distribution and the order parameter symmetry, and then generate the predicted $I_cR_n(B)$ patterns. This procedure is unfortunately not unique.

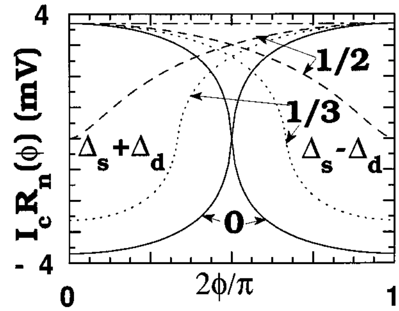

FIG. 2. Plots of $F_{AB}(\phi)$ [Eq. (7)] for $\Delta_s\pm\Delta_d$, with $\Delta_1=1$ meV, $\Delta_{20}=10$ meV, and $\alpha=0$ (solid curves), 1/3 (dotted curves), 1/2 (dashed curves), and 1 (dot-dashed line).

We assume the HTCS order parameter $\Delta_2(\phi)$ has $s\pm d_{x^2-y^2}$ symmetry, which may be written as

$$\Delta_2(\phi)=\Delta_{20}[\alpha\pm(1-\alpha)\cos(2\phi)], \tag{9}$$

where $0\leqslant\alpha\leqslant 1$ is the fraction of the maximum HTCS order parameter amplitude that arises from s-wave superconductivity. For simplicity, we assume the CS order parameter $\Delta_1=1$ meV and $\Delta_{20}=10$ meV throughout this manuscript.

In Fig. 2, we have plotted $F_{AB}(\phi)$ from Eq. (7), for $\alpha=0$, 1/3, 1/2, and 1. For clarity, we have included both signs in Eq. (9), corresponding to the $\Delta_s\pm\Delta_d$ states expected to be present in a twinned, orthorhombic crystal. In an untwinned

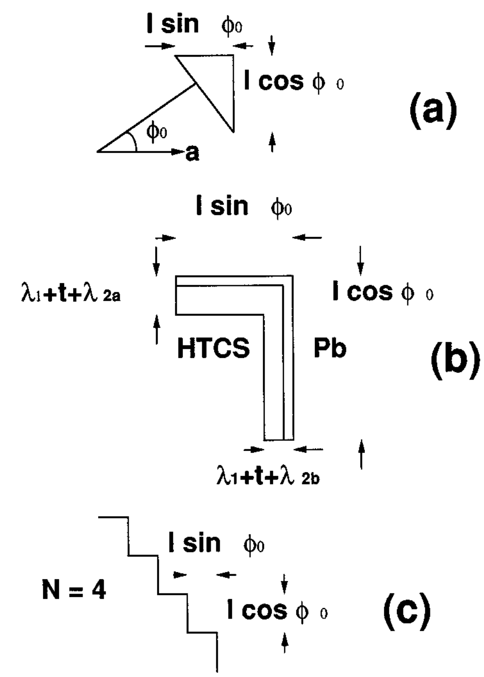

FIG. 3. (a) Schematic view of an idealized single ($N=1$) facet appropriate for the junction on the cleave plane normal to the angle ϕ_0 relative to the a axis, as in Fig. 1. (b) Blowup of the facet, illustrating the different effective field penetrations $d(0)$ and $d(\pi/2)$. (c) Schematic view of four equal facets.

crystal, only one of these states is expected, but the choice is arbitrary, based upon the ‘‘conventional wisdom.’’

B. Jagged cleave edges

In real layered materials, it is much easier to cleave the samples with a cleave plane normal to the sample *c* axis than to do so in any other direction. Nevertheless, samples of YBCO thin enough to allow for detwinning can be cut with the cleave plane normal to the ab plane, as assumed above. Thus, one can choose the angle ϕ_0, the normal to the cleave plane makes with the sample a axis, to be essentially arbitrary. Unfortunately, such cleave planes are usually faceted, forming many steps of a- and b-axis microdomain cleave planes. Upon cleaveage, the local structure of such microfaceting is not well controlled, and may be somewhat random. In Fig. 3(a), we have illustrated an idealized single facet obtained for a cleave plane normal to ϕ_0, with effective length ℓ, and effective domain edges $\ell\cos\phi_0$ and $\ell\sin\phi_0$, respectively. Fortunately, it appears possible to control the local variation of these microdomains by thermal annealing.[32] In the annealing process, the facets tend to become *regular*, with a periodic ladder structure of microfacets shown in Fig. 3(c). We thus treat theoretically the case of a regular array of microfacets. In addition, we assume the critical current between the CS and HTCS materials depends only upon the relative orientation of the order parameters with the cleave plane. This assumption may be particularly suspicious, as it is quite possible that the critical current may be different in the a and b directions in orthorhombic samples for reasons other than the order-parameter anisotropy. Some experiments suggest that oxygen deficiency can be different along different sample surface directions,[19,33] and such oxygen deficiency could lead to magnetic impurities at the sample surfaces, accounting for the observed zero-bias conductance peaks for a-axis YBCO/Pb junctions, which split in a magnetic field, but not for the zero-bias conductance *dips* in the c-axis YBCO/Pb junctions.[33] Such paramagnetic impurities at particular a-axis junction sites can lead to the associated changes in sign of the critical current in the Josephson junction at those locations, which would be completely unrelated to the order-parameter symmetry. For pedagogic purposes, however, we presently neglect both these and the spurious trapped flux complications, focusing upon the idealized situation.

For the idealized single facet pictured in Fig. 3(b), it is straightforward to obtain

$$eI_cR_n|_{N=1}=\frac{(Z^2(0)+Z^2(\pi/2)+2Z(0)Z(\pi/2)\cos\{\pi[\Phi(0)+\Phi(\pi/2)]/\Phi_0\})^{1/2}}{\ell(0)+\ell(\pi/2)}, \tag{10}$$

where $Z(\phi)=G(\phi)\ell(\phi)$ is given by Eqs. (4) and (6). This particular case is relevant to the uncleaved corner junction, with a built-in asymmetry of the junction widths $\ell(0)/\ell(\pi/2)$, such as was discussed by Ref. 12. However, for untwinned samples, there is an additional complicating feature of the inequivalence of the penetration depths along the two sample surfaces, which greatly complicates the $I_cR_n(B)$ pattern. This is shown by the solid curve in Fig. 4(a). We note that the curve is quite complicated, arising from the difference of the penetration depths along the two sides of the facet. Of course, the problem of flux pinned at the corners is notorious for this geometry, and can give spurious phase changes of π at the corners. Nevertheless, one can learn some interesting information from such a simple geometry on untwinned rectangular single crystals, by forming asymmetric junctions, such as pictured by the solid curves in Figs. 4 and 5, around two or more corners on the same sample, so that the relative sign of the s/d mixing of the supposed HTCS order parameter would be fixed. This would be most useful if the d-wave component of the order parameter were to be larger than the s-wave component (i.e., $\alpha<1/2$), such as in Fig. 5.

We now consider that the junction consists of a periodic array of $N\geqslant 1$ facets, such as pictured in Fig. 3(c). Assuming the magnetic vector potential is well behaved at the facet corners (i.e., that there is no trapped flux, for instance), we find

$$eI_cR_n|_N=eI_cR_n|_{N=1}\left|\frac{\sin\{N\pi[\Phi(0)+\Phi(\pi/2)]/\Phi_0\}}{N\sin\{\pi[\Phi(0)+\Phi(\pi/2)]/\Phi_0\}}\right|. \tag{11}$$

In Fig. 4, we have shown the resulting I_cR_n for the d-wave case $\alpha=0$, at junction angles $\phi_0=\pi/4$ and $\pi/8$, for $N=1$, 3, 10, and 30, respectively. Similar plots for the $\Delta_s+\Delta_d$ state with $\alpha=1/3$ and $\phi_0=\pi/8$ are shown in Fig. 5(b). From these plots, one can readily observe that it does not take a particularly large number of regularly spaced facets to completely modify $I_cR_n(B)$ from the single facet behavior. Quite generally, we find that for $N\geqslant 30$, the pattern obtained closely resembles the Fraunhofer diffraction pattern $I_cR_n\propto|\sin[\pi\Phi/\Phi_0]/[\pi\Phi/\Phi_0]|$, as in Eq. (4).

Hence, one should always obtain the standard pattern, but the *amplitude* will depend upon the angle ϕ_0 and the s-wave order-parameter fraction α. For instance, from Fig. 4(a), $I_cR_n\rightarrow 0$, as expected from the perfect, straight junction formula, Eq. (4). Generally, the amplitude at $B=0$ differs from the smooth, perfect junction formed by a constant factor, equal to the ratio of the lengths of the junctions in the perfect and faceted cases. In short, all of the unusual behaviors predicted for the $N=1$ cases are washed out in the periodic array of N facets, as long as $N\geqslant 30$.

III. DISK-SHAPED SINGLE CRYSTALS

We now assume the HTCS can be formed into a circular disk of radius r_0 and thickness t_0, with the crystal c axis

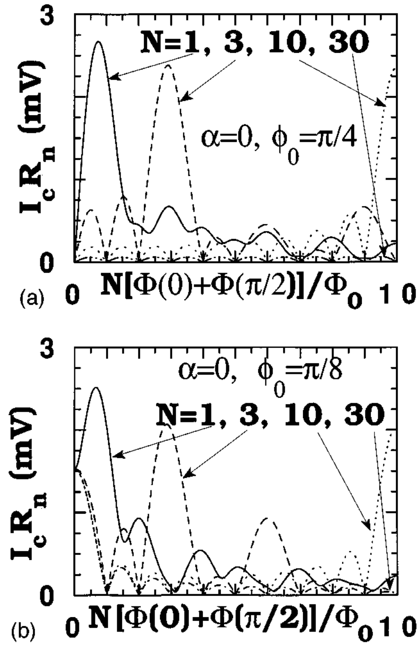

FIG. 4. Plots of I_cR_n vs $N[\Phi(0)+\Phi(\pi/2)]/\Phi_0$ from Eqs. (9) and (10) for the d-wave case $\alpha=0$ with $N=1$ (solid line), 3 (dashed line), 10 (dotted line), and 30 (dash-dotted line). See text. (a) $\phi_0=\pi/4$. (b) $\phi_0=\pi/8$.

normal to the disk face. At the present, two techniques for the formation of HTCS disks have already been attempted, by grinding[26] and by laser cutting.[24] We assume that improved techniques will eventually be able to make near-perfect disks, with ab faceting mainly on an atomic scale. In the previous section, we showed that regular faceting of the

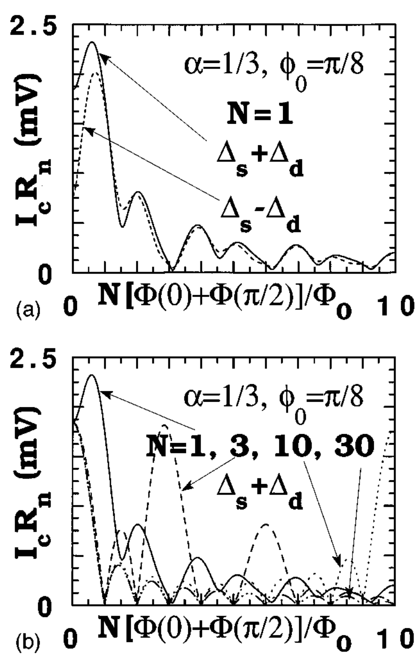

FIG. 5. Plots of I_cR_n vs $N[\Phi(0)+\Phi(\pi/2)]/\Phi_0$ for $\alpha=1/3$, and $\phi_0=\pi/8$. (a) $N=1$. Solid curve: $\Delta_s+\Delta_d$. Dashed curve: $\Delta_s-\Delta_d$. (b) $\Delta_s+\Delta_d$ only, but $N=1$ (solid line), 3 (dashed line), 10 (dotted line), and 30 (dash-dotted line).

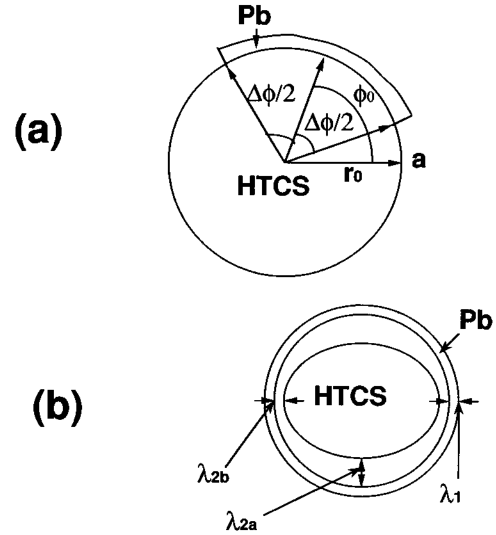

FIG. 6. (a) Schematic top view of the Josephson junction of angular arc $\Delta\phi$ centered at ϕ_0 relative to $\hat{a}$, formed on the edge of an HTCS disk of radius r_0. (b) Schematic diagram of the effective junction thickness $d(\phi)$ from Eq. (11).

Josephson junction is not qualitatively different from perfectly smooth straight junctions. In the disk-shaped case, the facets produced after annealing are expected to vary in a systematic fashion with the minimum height of a facet being a unit cell parameter (a or b).

On the edge of the disk, an SIS' junction is prepared with a CS, such as Pb, as pictured in Fig. 6. The thickness of the junction is taken to be t, with total effective field penetration thickness $\Delta r(\phi)$ given by $d(\phi)$ in Eq. (1). It is straightforward to derive Eq. (2), by assuming the field is normal to the disk (which is strictly speaking only true in certain experimental configurations, as discussed in the following). In cylindrical coordinates, the effective area of the junction is the area enclosed by an integration path consisting of (1) the circular arc of radius $r_0+t+\lambda_1$ inside the CS outside the disk, (2) the inward radial path across the junction, (3) the (elliptical) path a distance $r_0-\lambda_{2ab}(\phi)$ from the center of the HTCS disk, and (4) the outward radial path from the disk to the CS. Note that the path inside the disk is circular for $\lambda_{2a}=\lambda_{2b}$, but is otherwise elliptical for untwinned, orthorhombic single crystals, as pictured in Fig. 6(b). In addition, the ϕ dependence of $\lambda_{2ab}(\phi)$ is as given in Eq. (2), since the integration paths are essentially perpendicular to the radial direction. We have derived Eq. (2) for this disk by solving either for the field or current distribution in a long cylinder in cylindrical coordinates, and by assuming $r_0 \gg \lambda_{2ab}(\phi)$. In this limit, the field and screening currents decay exponentially in from the disk edge, with decay length precisely given by Eq. (2).

For heavily twinned disks, or for tetragonal single crystals, one can assume Δr independent of ϕ. Otherwise, for orthorhombic, untwinned single crystals, $\lambda_{2ab}(\phi)$ is as given by Eq. (2). The junction is assumed to be centered at the angle ϕ_0 relative to the a axis, and extends along the disk edge between the angles $\phi_0-\Delta\phi/2$ and $\phi_0+\Delta\phi/2$, relative to the HTCS a axis, as shown in Fig. 6(a). In cylindrical coordinates, the magnetic induction at the junction is taken to be $\mathbf{B}=B\hat{z}$, and the magnetic vector potential at the radius r can be taken to be $\mathbf{A}=\frac{1}{2}Br\hat{\boldsymbol{\phi}}$. The flux $\Phi(\phi)$ in the junction is then

$$\Phi(\phi)=Br_0 d(\phi)\Delta\phi, \tag{12}$$

with $d(\phi)$ given by Eq. (1). The critical current in the junction is then given by

$$eI_cR_n=\left|\int_{\phi_0-\Delta\phi/2}^{\phi_0+\Delta\phi/2}\frac{d\phi}{\Delta\phi}F_{AB}(\phi)\exp[2i\pi\Phi(\phi)\phi/(\Delta\phi\Phi_0)]\right|, \tag{13}$$

where $F_{AB}(\phi)$ is given by Eq. (7), and $\Phi(\phi)$ is given by Eq. (12). As for the straight cleave, the junction should be designed so that $r_0\Delta\phi<\lambda_J\approx 1$ mm. We have also assumed a critical current distribution that varies over the junction only because of the angular dependence of the order parameter, according to $F_{AB}(\phi)$ in Eq. (7). Any additional variation in the critical current density arising from trapped flux, chemical inhomogeneities, etc., will modify the form of $F_{AB}(\phi)$ in Eq. (13).

In Figs. 7, 8, and 9, we have presented plots of detailed calculations based upon Eq. (13). In these figures, we have chosen $\Delta_1=1$ meV, $\Delta_{20}=10$ meV, $\lambda_{2a}/\lambda_{2b}=\sqrt{2}$, $\lambda_{2a}=0.75d(\pi/2)$, $\Delta\phi=\pi$, and the s-wave fraction $\alpha=0$, 1/3, 1/2, and 1. These values are consistent with YBCO/Pb junctions. The only differences between Figs. 7, 8, and 9 are the signs of the mixing, $\Delta_s\pm\Delta_d$, and the locations of the centers of the junction, which are at $\phi_0=0$, $\pi/4$, and $\pi/2$, respectively. Note that we have assumed an *untwinned* single-crystal disk with $\lambda_{2a}\neq\lambda_{2b}$, so that the effective ''flux'' $\Phi(\phi)$ depends upon ϕ. For $\phi_0=0$, $\pi/2$, the ϕ dependence of $\Phi(\phi)$ is symmetric about ϕ_0, so that I_cR_n vanishes at specific flux values. For $\phi_0=\pi/4$, however, this is not the case *even* for the purely s-wave case $\alpha=1$, due to the anisotropy in the penetration depth. For comparision purposes, we choose to plot these figures as functions of $\pi\Phi(0)/\Phi_0$.

We have examined the range of behaviors expected for the disk, by varying ϕ_0 and $\Delta\phi$ for $\alpha=0$, 1/3, 1/2, and 1. For small $\Delta\phi$ values, one generally obtains the standard Fraunhofer diffraction pattern $I_cR_n\propto|\sin[\pi\Phi(\phi)/\Phi_0]/[\pi\Phi(\phi)/\Phi_0]|$.The only difference between curves arises from the amplitude of such patterns, which becomes vanishingly small at the positions of possible nodes. This situation is thus very similar to that obtained for the straight cleave, discussed in Sec. II. However, for small $\Delta\phi$, it might be experimentally difficult to distinguish between a small signal arising from a node and that arising from a bad junction. If the disk were not perfectly uniform in junction-forming capability, such problems of interpretation might be difficult to overcome for small $\Delta\phi$ junction values.

For larger $\Delta\phi$ values, one has to be sure that the junction really is formed over the entire edge region assumed to lie within $\Delta\phi$. As $\Delta\phi$ increases, one will need to take increasing amounts of experimental care to assure such uniformity. However, the payoff is that the $I_cR_n(B)$ patterns become increasing distinctive, at least for small magnetic field strengths. Let us consider a d-wave superconductor with $\Delta\phi=\pi/2$. In this case, with the order-parameter amplitude maxima positioned along the a and b directions, one obtains a large Fraunhofer signal for $\phi_0=0$, $\pi/2$, but a vanishing signal for $\phi_0=\pi/4$, a nodal position. One could do a large number of experiments with such a configuration, performing detailed fits to the calculations obtained by evaluating Eq. (13). From a significant number of such junctions, it ought to be possible to determine the symmetry of the order parameter.

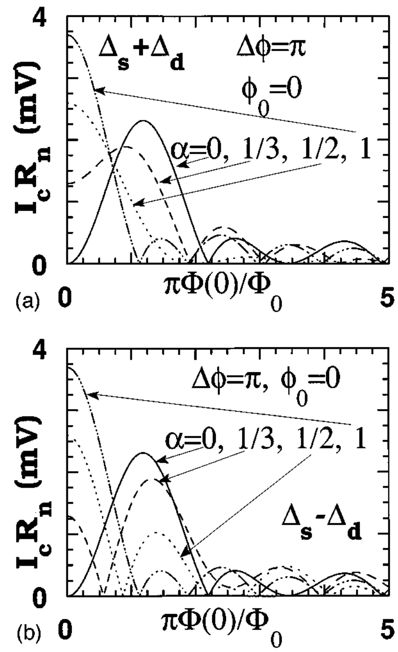

FIG. 7. Plots of I_cR_n vs $\pi\Phi(0)/\Phi_0$ from Eq. (12) for the disk junction with $\Delta\phi=\pi$, $\phi_0=0$, and $\alpha=0$ (solid line), 1/3 (dashed line), 1/2 (dotted line), and 1 (dash-dotted line). (a) $\Delta_s+\Delta_d$.(b) $\Delta_s-\Delta_d$.

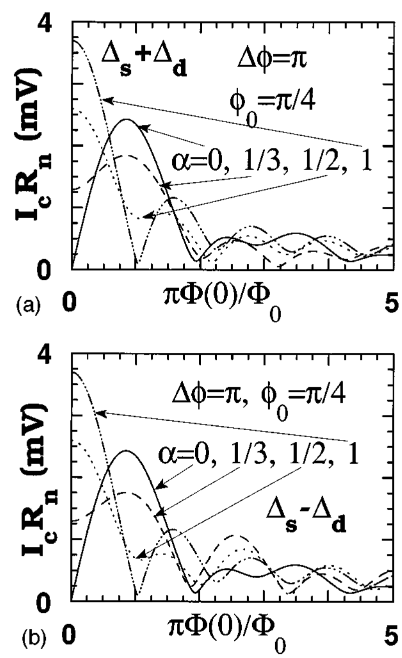

FIG. 8. Same plots as for Fig. 7, except $\phi_0=\pi/4$. (a) $\Delta_s+\Delta_d$. (b) $\Delta_s-\Delta_d$.

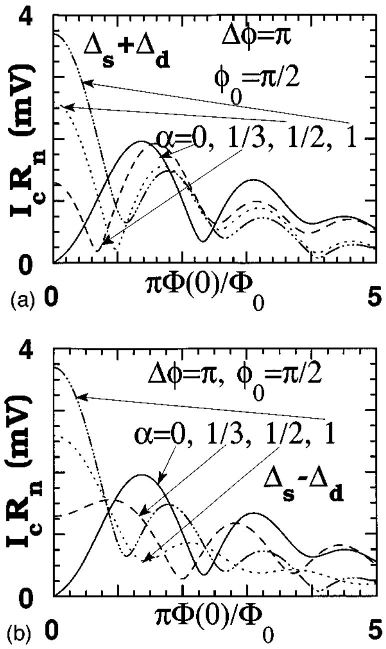

FIG. 9. Same plots as for Figs. 7 and 8, except $\phi_0=\pi/2$. (a) $\Delta_s+\Delta_d$. (b) $\Delta_s-\Delta_d$.

By far the most reliable method, however, occurs for $\Delta\phi=\pi$, as pictured in Figs. 7, 8, and 9. For these figures, it is readily seen that the behavior at small $\Phi(0)/\Phi_0$ is both *distinctive* for different s-wave fractions α, and also remarkably *insensitive* to the central location angle ϕ_0 of the junction. The pure d-wave case $\alpha=0$ *always* exhibits a node at $\Phi=0$, independent of ϕ_0, and the largest maxima are adjacent to the central node at $B=0$. For the case $\alpha=1/3$ of a predominately d-wave superconductor, $I_cR_n(B)$ exhibits two types of behavior. In the first case, it exhibits a nonvanishing dip at $B=0$, with the largest maxima on either side of the dip. In the second type of behavior, there is a central maximum, followed by adjacent nodes or very small minima, and subsequently followed by the largest maxima. This behavior is most prominent for the $\Delta_s+\Delta_d$ state at $\phi_0=\pi/2$, and for the $\Delta_s-\Delta_d$ state near $\phi_0=0$. In contrast, the pure- and predominately-s-wave superconductor junctions give rise to low-$\Phi(0)$ behavior of I_cR_n that is also fairly insensitive to ϕ_0. These cases always give rise to the largest maximum being at $B=0$, and the ratio of the central maximum to the adjacent maxima increases with increasing α.

On the other hand, the large-Φ behavior of each of the curves appears to depend strongly upon all of the parameters. Such details can be useful in an accurate fitting of the $I_cR_n(B)$ patterns, provided that the material parameters Δ_1, Δ_{20}, λ_1, λ_{2a}, and λ_{2b} are all accurately known. Thus, if the experimenter could prepare a series of untwinned disk-shaped junctions centered at different ϕ_0 values, he or she should be able to determine the relative amount of s/d mixing of the order parameter in the orthorhombic HTCS.

IV. DISCUSSION

Trapped flux can be a major concern in these and all previous experiments purporting to determine the symmetry of the order parameter. In recent junctions formed along the ab edges of thick single crystals of YBCO, the unreliable $I_c(B)$ patterns obtained with $\mathbf{B}\perp\hat{c}$ indicated that trapped flux lying in the ab planes was nearly impossible to remove.[3] More recently, Kirtley made SQUID microscope studies of the edge of a nearly detwinned single crystal of nominally zero-field-cooled YBCO.[34] He found a large amount of trapped flux lying in the ab plane. We thus expect trapped flux to complicate the analysis of the experiments proposed here. However, the experimental configurations proposed here are different, and in some ways superior to those studied previously.

The corner junctions of Ref. 12 are particularly susceptible to problems of trapped flux, since flux is preferentially pinned at the corners,[21] which are the junction centers. When the flux is trapped in the junction center, the $I_c(B)$ pattern can vanish at $B=0$. For example, this has been shown for monopole vortices[35] pinned in the centers of SNS junctions,[36] and for one or more flux quanta[37] trapped in an annular Josephson junction.[38] It was also shown for a c-axis YBCO/Pb junction, when a single flux quantum was trapped in the junction and subsequently removed by thermal cycling.[3]

For the geometries considered here, however, the positions of the trapped flux will generally not be dictated by the sample geometry, and are thus expected to arise from local, random, chemical, and/or physical disorder. Thus, the trapped flux will primarily modify the large-B behavior of I_cR_n, not the small-B behavior. The experimenter then has at least two options. First, he or she can cycle the junction through the T_c of the HTCS a number of times, in order to see if the results on the same junction are reliable. Second, he or she can make a number of nominally identical junctions.

If the behavior at $B=0$ is consistent, the experimenter can probably rely on the results. Otherwise, the experimenter may have to make further attempts to either remove or understand the effects of the trapped flux. In any event, by performing the experiment on a number of such untwinned disk samples, the experimenter should be able to obtain rather good statistics, which can be used to offset the nearly random occurrences of trapped flux. Hence, this $\Delta\phi=\pi$ geometry allows the experimenter to eliminate the effects of trapped flux *experimentally*, not merely by guessing what it will do in some (but not all) circumstances.

The theoretical analysis presented here is of course greatly simplified. For example, real HTCS's are complicated materials. In some samples such as YBCO, the electronic properties involve both chains and planes. In particular, surface states[39] have been shown to give a possible explanation of the gapless single-particle density-of-states curves reproducibly obtained in tunneling data. It is not yet understood how such surface states might affect the Josephson-junction I_cR_n values, but their role could be significant.[29] In addition, there appear to be significant materials problems in forming Josephson junctions on materials other than YBCO, and actual SIS' junctions on the edges of YBCO have only very recently been produced.[3] Nevertheless, the geometry we have proposed here is about as free of trapped flux problems as can reasonably be expected. Although corner experiments on untwinned single crystals

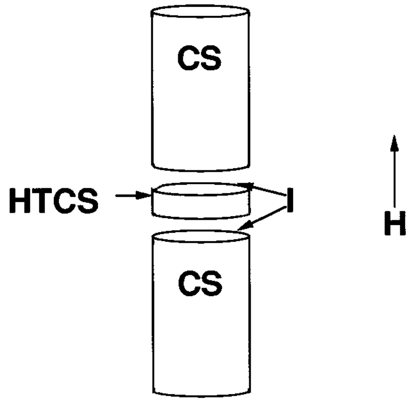

FIG. 10. Schematic diagram of proposed method to reduce demagnetization effects of the disk in a perpendicular field. The disk is sandwiched between two thin insulators and conventional superconducting cylinders with cross sections identical to the HTCS disk.

could also be employed to study the s-wave fraction α, such junctions are inherently subject to flux trapping at the statistically nonrandom corner locations.

Finally, we propose that the measurements on the disk and/or straight cleave junctions be carried out in the experimental configuration pictured schematically in Fig. 10 for the disk. Both on top of and below the HTCS sample are placed large CS objects of the same geometrical cross section. These CS materials are separated from the HTCS by insulators, which are thick enough to eliminate any Josephson tunneling between them and the HTCS (which has now been firmly established to occur along the c axis), but not too thick to allow for significant magnetic field penetration into the insulating regions. Thus, the insulators should be roughly on the order of but slightly less than a CS penetration depth in thickness. For this configuration, the magnetic field will be nearly parallel to the Josephson junctions under study, and a more accurate fit of the data to the theory can be made.

ACKNOWLEDGMENTS

The author would like to thank B. W. Veal and A. P. Paulikas for helpful discussions. This work was supported by the U. S. Department of Energy under Contract No. W-31-109-ENG-38.

[1] A. G. Sun, D. A. Gajewski, M. B. Maple, and R. C. Dynes, Phys. Rev. Lett. **72**, 2267 (1994).
[2] A. G. Sun, S. H. Han, A. S. Katz, D. A. Gajewski, M. B. Maple, and R. C. Dynes, Phys. Rev. B **52**, R15 731 (1995).
[3] A. G. Sun, A. Truscott, A. S. Katz, R. C. Dynes, B. W. Veal, and C. Gu, Phys. Rev. B **54**, 6734 (1996).
[4] A. S. Katz, A. G. Sun, R. C. Dynes, and K. Char, Appl. Phys. Lett. **66**, 105 (1995).
[5] R. Kleiner, A. S. Katz, A. G. Sun, R. Summer, D. A. Gajewski, S. H. Han, S. I. Woods, E. Dansker, B. Chen, K. Char, M. B. Maple, R. C. Dynes, and John Clarke, Phys. Rev. Lett. **76**, 2161 (1996).
[6] P. Chaudhari and S.-Y. Lin, Phys. Rev. Lett. **72**, 1084 (1994).
[7] C. C. Tsuei, J. R. Kirtley, C. C. Chi, L.-S. Yu-Jahnes, A. Gupta, T. Shaw, J. Z. Sun, and M. B. Ketchen, Phys. Rev. Lett. **73**, 593 (1994); C. C. Tsuei, J. R. Kirtley, M. Pupp, J. Z. Sun, L.-S. Yu-Jahnes, C. C. Chi, A. Gupta, and M. B. Ketchen, J. Phys. Chem. Solids **56**, 1787 (1995).
[8] C. C. Tsuei, J. R. Kirtley, M. Rupp, J. Z. Sun, A. Gupta, M. B. Ketchen, C. A. Wang, Z. F. Ren, J. H. Wang, and M. Bhushan, Science **271**, 329 (1996).
[9] A. Mathai, Y. Gim, R. C. Black, A. Amar, and F. C. Wellstood, Phys. Rev. Lett. **74**, 4523 (1995).
[10] D. A. Wollman, D. J. Van Harlingen, W. C. Lee, D. M. Ginsberg, and A. J. Leggett, Phys. Rev. Lett. **71**, 2134 (1993).
[11] D. Brawner and H. R. Ott, Phys. Rev. B **50**, 6530 (1994).
[12] D. A. Wollman, D. J. Van Harlingen, J. Giapintzakis, and D. M. Ginsberg, Phys. Rev. Lett. **74**, 797 (1995).
[13] R. A. Klemm, Phys. Rev. Lett. **73**, 1871 (1994).
[14] Anna Mathai, Ph.D. thesis, University of Maryland, 1995.
[15] J. Clarke and T. A. Fulton, J. Appl. Phys. **40**, 4470 (1969).
[16] H. Hilgenkamp, J. Mannhart, and B. Mayer, Phys. Rev. B **53**, 14 586 (1996).
[17] D. J. Miller, T. A. Roberts, J. H. Kang, J. Talvacchio, D. B. Buchholz, and R. P. H. Chang, Appl. Phys. Lett. **66**, 2561 (1995).
[18] M. B. Field, A. Pashitski, A. Polyanskii, D. C. Larbalestier, A. S. Parikh, and K. Salama, IEEE Trans. Appl. Supercond. **AS-5**, 1631 (1995).
[19] S. E. Babcock, X. Y. Cai, D. C. Larbalestier, D. H. Shin, N. Zhang, H. Zhang, D. L. Kaiser, and Y. Gao, Physica C **227**, 183 (1994).
[20] Y. Gim, A. Mathai, R. C. Black, A. Amar, and F. C. Wellstood (unpublished).
[21] R. A. Klemm (unpublished).
[22] T. Schuster, H. Kuhn, and M. V. Indenbom, Phys. Rev. B **52**, 15 621 (1995).
[23] M. K. Hasan, S. J. Park, and J. S. Kouvel, Physica C **254**, 323 (1995).
[24] R. A. Klemm, A. M. Goldman, A. Bhattacharya, J. Buan, N. E. Israeloff, C. C. Huang, O. T. Valls, J. Z. Liu, R. N. Shelton, and U. Welp, Phys. Rev. Lett. **77**, 3058 (1996); A. M. Goldman (private communication).
[25] J. Buan, B. P. Stojkovic, N. E. Israeloff, A. M. Goldman, C. C. Huang, O. T. Valls, J. Z. Liu, and R. Shelton, Phys. Rev. Lett. **72**, 2632 (1994).
[26] U. Welp (private communication).
[27] F. Yu, M. B. Salamon, A. J. Leggett, W. C. Lee, and D. M. Ginsberg, Phys. Rev. Lett. **74**, 5136 (1995); **75**, 3028 (1995).
[28] V. Ambegaokar and A. Baratoff, Phys. Rev. Lett. **10**, 486 (1963); **11**, 104 (1963).
[29] M. Ledvij and R. A. Klemm, Phys. Rev. B **51**, 3269 (1995); **52**, 12 552 (1995).
[30] B. D. Josephson, in *Superconductivity*, edited by R. Parks (Dekker, New York, 1969), p. 441.
[31] M. Tinkham, *Introduction to Superconductivity*, 2nd ed.

(McGraw-Hill, New York, 1996), p. 217.

[32] B. W. Veal (private communication).

[33] J. Lesueur, L. H. Greene, W. L Feldmann, and A. Inam, Physica C **191**, 325 (1992); M. Covington and L. H. Greene, in *Spectroscopic Studies of Superconductors*, edited by I. Bozovic and D. van der Marel [Proc. SPIE **2696**, 394 (1996)].

[34] J. R. Kirtley, *Proceedings of the 21st International Conference on Low Temperature Physics* [Czech. J. Phys. **46** Suppl. S6 (to be published)].

[35] S. L. Miller K. R. Biagi, J. R. Clem, and D. K. Finnemore, Phys. Rev. B **31**, 2684 (1985).

[36] O. B. Hyun, J. R. Clem, and D. K. Finnemore, Phys. Rev. B **40**, 175 (1989).

[37] I. V. Vernick, S. Keil, A. V. Ustinov, N. Thyssen, T. Doderer, H. Kohlstedt, and R. P. Huebener, *Proceedings of the 21st International Conference on Low Temperature Physics,* Prague, 1996 [Czech. J. Phys. **46**, Suppl. S2, 649 (1996)].

[38] A. Davidson, B. Dueholm, B. Kryger, and N. F. Pedersen, Phys. Rev. Lett. **55**, 2059 (1985).

[39] S. H. Liu and R. A. Klemm, Phys. Rev. B **52**, 9657 (1995).